An investigation of the impact response of European ash and sycamore maple

Mojtaba Hassan Vand *
Department of Wood Science and Wood Technology, Mendel University, Zemědělská 1665, Brno, Czech Republic. Email: mojtaba.vand@mendelu.cz

Jan Tippner †
Department of Wood Science and Wood Technology, Mendel University, Zemědělská 1665, Brno, Czech Republic. Email: jan.tippner@mendelu.cz

(Received 7 May 2026)

Abstract: European ash (*Fraxinus excelsior* L.) and sycamore maple (*Acer pseudoplatanus* L.) have long historical applications in structural components requiring high impact resistance, yet a detailed characterization of their full-field dynamic strain behavior remains limited. This study investigates the impact bending responses of both species using three-point drop-weight impact tests integrated with high-speed recording (10,000 frames per second) and the digital image correlation (DIC) method. The distinct and interactive effects of moisture content (MC) and growth-ring orientation (GO) were evaluated across key mechanical metrics: maximum deflection of the beam up to crack initiation, maximum normal strain, maximum reaction force (F_{max}), total absorbed energy, and impact bending strength (IBS). The IBS of ash and maple were 6.3 and 4.5 J/cm², respectively, while their maximum deflection was 8.5 and 8.6 mm, respectively. Two-way ANOVA revealed highly species-specific sensitivities to environmental and structural factors. For European ash, unlike F_{max}, other results such as maximum deflection, maximum strain, total absorbed energy, and IBS were not significantly altered by MC or GO. Conversely, sycamore maple exhibited highly isotropic behavior regarding GO, but it showed to be dependent on the MC. MC significantly enhanced the maximum deflection and maximum normal strain of maple, while triggering a severe 64% reduction in F_{max}. The force-time charts of the tests showed a distinct structural transition from a rigid, brittle fracture mode at low moisture levels to a highly dampening, ductile deformation mode once exceeding the fiber saturation point (FSP). These findings highlight the strong effect of species type on the impact mechanics, providing a robust experimental dataset essential for developing and validating analytical and finite element models.

Keywords: Ash; Maple; Impact test; Digital image correlation method; Three-point bending; High-speed camera; Moisture content; Growth-ring orientation.

Introduction

European ash, or common ash (*Fraxinus excelsior* L.), is a vital species for the functioning and conservation of forests throughout Europe, typically growing as an admixed tree species and rarely achieving dominance (Pautasso et al. 2013). This species thrives on fertile, well-drained soils with a neutral pH and is scattered across various forest communities (Dobrowolska et al. 2011). It can grow from lowland fields and meadows to medium-height mountains, as long as its water requirements are met, and it can reach heights of up to 40 m and a diameter of 1 m (Tudor et al. 2011). Ash is highly sensitive to fire and freezing temperatures; furthermore, it exhibits one of the highest sensitivities to drought (Thomas 2016).

Ash wood's remarkable strength, flexibility, impact resistance, and springiness make it an exceptional material for sports equipment items like baseball bats, tennis rackets, polo shafts, and hockey sticks (Clauß et al. 2014; Boshier et al. 2005). In fact, ash has a significant place in baseball history, largely due to its superior impact strength for bat production (Fortin-Smith et al. 2016a). Compared to many other common wood species, ash boasts relatively high mechanical properties, including excellent strength and fracture toughness (Niemz et al. 2014). Its impact bending strength (IBS) is one of the highest among common species (Borůvka et al. 2020). The exceptional performance of ash under impact loadings has naturally drawn researchers and designers to explore its use in various impact-related applications. Studies have also utilized techniques such as finite element method modeling to predict and optimize the response of ash and other types of wood to impact (Fortin-Smith et al. 2016b, 2018).

* Corresponding author
† Society of Wood Science & Technology member

The sycamore maple (*Acer pseudoplatanus* L.) is a large hardwood tree characterized by a broad, domed crown and a strong root system which can reach heights of 30–35 m (Pasta et al. 2016). This fast-growing species is common in many European forests, though it rarely forms pure stands, typically growing in mixture with other species (Vacek et al. 2018). Sycamore maple can thrive in full sun or partial shade and shows no sensitivity to soil pH, adapting well to a wide range of soil types (Gilman and Watson 1993). It grows successfully in mixed deciduous forests, showing resilience to diverse ecological conditions, saline or eroded soils, and climate shifts (Iliev et al. 2022). Furthermore, it has no difficulty colonizing coarse scree or colluvium on slopes (Bodziarczyk and Lesiński 2011).

Due to its hardness and ease of processing, maple wood is suitable for a range of applications, including furniture, carpentry, flooring, and molding (Sedlar et al. 2021). Alongside ash, maple is also valued for its high IBS (Campshure et al. 2020). Maple wood can have wavy fibers, which makes it particularly favored for the backs of violins and other stringed musical instruments, a practice that luthiers have employed for centuries (Dinulica et al. 2023). The application of maple wood, according to some researchers, could be further expanded and optimized through progressive improvements in data concerning its mechanical properties (Sonderegger et al. 2013).

Given their widespread use, wood and wooden products are frequently subjected to various types of loading, including impacts (Polocoșer et al. 2017). Wooden structures can constantly experience impacts due to common scenarios of different types of tasks, such as automobile crashes affecting wooden guardrails (Gutkowski et al. 2007), natural hazards damaging wooden buildings (Yamada et al. 2018; Turnbull-Grimes et al. 2010), packaging applications (Liu and Chen 2010), or even simple domestic incidents (Acuña et al. 2020). The viscoelastic nature of wood means its response varies significantly with different loading types, from creep to impact. Consequently, various testing methods have been developed to account for these differences in mechanical behavior under varying loading rates (Polocoșer et al. 2018). By studying and understanding wood's mechanical behavior under impact, we can use it more efficiently, broaden its applications, and reduce the risk of potential damage (Baumann et al. 2021).

One of the most common impact tests for wood is the three-point impact bending test. While relatively simple to set up and execute, its analysis is complex due to the simultaneous occurrence of tension, compression, and shear forces (Sahraoui and Lataillade, 1998). This test determines the IBS, which represents the work required to break a specimen, independent of its dimensions (Borůvka et al. 2020). IBS can be measured by dividing the absorbed energy of the impact by the beam's cross-sectional area at its center (Moreira et al. 2017). By altering various parameters and characteristics of the wood samples, this test can identify factors influencing wood's impact behavior (Hassan Vand and Tippner 2023). Both the structural and mechanical properties of wood, along with environmental conditions, can significantly influence its mechanical response (Glass and Zelinka 2021), including its impact response (Kretschmann 2010). Key environmental factors include moisture content (MC), temperature, and any modification applied to the wood.

Due to the chaotic nature of impact loadings, it is preferable to assess desired parameters using non-contact methods (Bragov et al. 2020). One of the most effective techniques for measuring the deformation and motion of objects during tests is digital image correlation (DIC). This method provides comprehensive information about all points of a specimen under examination (Sutton et al. 2009). Although DIC is relatively new to wood testing (Choi et al. 1991), its adoption has been rapid, making it now a common tool for assessing various types of static wood tests and for validating wood modeling methods (Keunecke et al. 2012). To efficiently measure deformations during dynamic tests, DIC requires integrating high-speed camera equipment, enabling the capture of deformations over extremely brief time intervals between successive images (Olmedo et al. 2015; Polocoșer et al. 2016; Hassan Vand et al. 2024). Prior to the advent of DIC, high-speed cameras were primarily used to determine the hammer's speed before and after impact and, consequently, to measure the energy imparted (Gerhards 1977).

Despite the fact that the ash and maple are commonly used woods with a long history of application in higher impact uses, a clear impact-related study with high-speed equipment was needed to see how internal deformation can lead to failure. Wood as a building material or as a part of the living trees can be affected by impacts, which should be controlled to prevent financial losses and casualties. For controlling the impact response and improving safety, a comprehensive study of the impact response of these species is required. This article comprehensively details the mechanical behavior of European ash and sycamore maple under impact loading, utilizing robust and suitable equipment to determine the effect of MC and growth-ring orientation (GO). This research provides information on these species' mechanical responses to impacts, including deflection, internal normal strain of specimens,

reaction loads, the work required for specimen failure, IBS, and shear strains at the neutral axis. The detailed deflection and strain distribution data presented in this paper can serve as a valuable criterion for validating various modeling methods for these wood species. To assess the influence of wood's MC on its impact behavior, these tests were conducted on specimens at two distinct MC levels.

Materials and methods

Samples with dimensions of 20 × 20 × 300 mm (radial × tangential × longitudinal) were cut from wood planks of European ash and sycamore maple from the South Moravian region in the Czech Republic. After preparation, every specimen was inspected visually for knots and defects, and those that did not meet the criteria were discarded. A total of 76 specimens were retained for testing, with 46 samples of ash wood and 30 samples of maple (see Table 1). The specimens of each species were divided into two groups: the lower moisture content (LMC) and the high moisture content (HMC) groups. The LMC samples were stored in a condition of 20°C and 65% relative humidity until their MC stabilized at approximately 11%. The HMC specimens were left under water for 2 d, then stored in sealed chambers with high level of MC above the water level for around 3 d, so that their MC steadily surpassed the fiber saturation point (FSP). The specimens were removed from their compartments only briefly before the tests to prevent moisture loss. Half of each group was tested in a way that the GO of the specimens was parallel to the direction of the hammer's movement. For the remaining specimens, the GO was positioned perpendicular to the direction of the hammer's movement. However, some studies showed that the GO has a negligible effect on certain aspects of the impact response of wood (Hassan Vand et al. 2024a, 2024b; Hassan Vand and Tippner 2023). Following testing, the specimens were placed in a drying oven at 103°C for 48 h to remove all moisture, enabling the determination of their oven-dry weight and exact MC.

To prepare the specimens, they were painted with a black-and-white random speckled pattern to improve the accuracy of the video extensometer and DIC (Pan et al. 2009). Just before the tests, the dimensions and weights of the specimens were measured. The tests were conducted at room temperature (≈20°C) in accordance with standards ČSN 490115 (Czech Technical Standard 1979), Wood: Determination of ultimate strength in flexure tests, and ČSN 490117 (Czech Technical Standard 1979), Wood: Impact strength in flexure. The tests were performed using a DPFest 400 drop-weight impact testing machine (Labortech s.r.o., CZ) with a displacement resolution of 10^{-5} m and a sampling frequency of 1 MHz. The reaction force was measured by an HBM force sensor from the CFTplus series (Hottinger Brüel & Kjaer, Austria). The weight of the hammer and its release height were 9.05 kg and 815.7 mm. This condition made the impact velocity 4 m/s, with 72.4 J of energy. Figure 1 shows a schematic of the specimens and clamps.

The samples were symmetrically positioned on two lower cylindrical support grips spaced 240 mm apart between their centerlines. Both the lower support grips and the upper impact hammer share identical geometric profiles, of a semi-cylindrical contact surface with a 15 mm radius and a lateral depth of 20 mm to match the specimen width. The upper impact hammer is aligned precisely at the mid-span (120 mm from each

Table 1. The physical and mechanical properties of the specimens and their test results. The median and CV% are in parentheses.

	Ash LMC	Ash HMC	Maple LMC	Maple HMC
MC (%)	11.0 (0.6)	55.5 (8.5)	10.55 (1.6)	62.2 (13.3)
Number of samples	35	11	15	15
Radial (mm)	20.1 (0.6)	20.9 (1.0)	20.1 (1.0)	20.6 (0.5)
Tangential (mm)	20.2 (0.7)	22.2 (0.8)	20.1 (0.7)	21.2 (0.8)
Length (mm)	300	300	300	300
Weight (g)	86.2 (3.1)	121.5 (5.3)	77.0 (2.1)	114.8 (5.1)
0% MC Weight (g)	77.5 (3.0)	77.2 (3.9)	70.1 (3.2)	69.9 (1.8)
Density (kg/m^3)	708.8 (3.2)	870.7 (6.1)	642.3 (2.0)	869.3 (5.0)
Max Deflection (mm)	8.5 (8.4)	8.2 (18)	8.6 (15.4)	9.1 (26.6)
Max Strain (–)	0.01266 (8.8)	0.01253 (16)	0.01465 (19.5)	0.01944 (23.4)
Max Force (N)	6899.5 (7.8)	5775.8 (13.7)	8967.8 (12.8)	3200.0 (12.2)
Absorbed Energy (J)	25.7 (16.4)	27.4 (18.0)	18.1 (19.2)	22.6 (37.8)
IBS (J/cm^2)	6.3 (17.0)	5.8 (18.0)	4.5 (19.5)	5.1 (37.9)

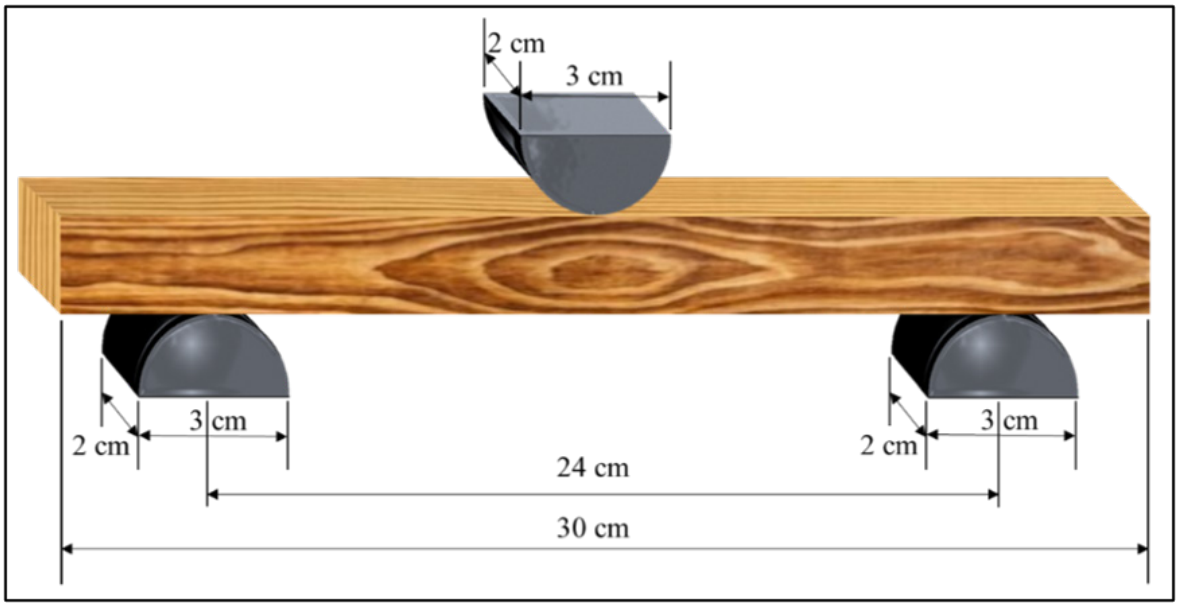


Figure 1. Schematic illustration of the three-point drop-weight impact bending test, the specimen dimensions, support span, impact hammer position, and loading configuration.

support centerline). The primary direction of impact is vertically downward, perpendicular to the longitudinal axis of the specimen. This induces a bending-dominated stress state at the mid-span, resulting in tensile stresses along the bottom surface and compressive stresses along the top surface of the beam profile.

The testing machine provides force vs. time charts and the total absorbed energy for breaking the specimens by integrating the force vs. displacement curves. All data curves were filtered directly by the built-in system of the impact testing machine. The output of charts had similar pattern but with different location for peaks and troughs. Thus, in order to calculate the median force-time curve accurately, minor misalignments required a slight extension or compression of the time scale (around 10% of total length). The value and timing of the maximum peak force were identified for each test, and the curves were adjusted so that all force peaks aligned at a single point. This synchronization ensures that the peaks and troughs of all curves line up correctly without distorting the data shape. Once the curves were synchronized, the median response was calculated for each time step.

A high-speed recording camera, FASTCAM SA-X2 type 1000K-M2 (Photron Cameras, Japan) alongside a mounted Nikon Micro-Nikkor G lens with a focal length of 105 mm (Nikon Corporation, Japan), was placed 1 m away at a perpendicular angle from the thickness-by-width specimens' surface. The camera recorded the impacts at 10,000 frames per second as black-and-white images of the central regions of the specimens, with a resolution of 768 × 328 pixels.

The recorded images were processed using Vic-2D v. 2010 (Correlated Solutions Inc., USA) DIC software. A simple 1D scale calibration with reference target of the thickness of the specimen was performed to determine the conversion factor, and a Lagrangian strain formulation was used to calculate strain tensors. The displacement field was considered 3×3 and the filter size was 5×5 points. The software could determine all point deformations, providing normal and shear strain distributions, as well as deflections, from the onset of impact to crack initiation in the specimens. Specimen deflection was measured by tracking the y-axis displacement of the beam's lowest point along its horizontal symmetry line. The maximum normal strain was also measured at the points where cracks initiated, which happened in the maximum deflection of each individual specimen. However, to mitigate noise, a small region around each point was used for strain determination rather than a single point.

For presenting a strain distribution pattern, the strains were captured at times corresponding to a chosen deflection of 4 mm. The strain distributions with values closest to the median and exhibiting more symmetrical form were selected as the typical strain distribution patterns. Additionally, the shear strain of the points along a multilinear probe located on the neutral axis of the samples was measured. DIC identified the neutral axis itself as the set of points with zero normal strain

for the images before crack initiation. The error of the DIC for measuring deflection and normal strain were 0.0073 mm and 0.00044, respectively. DIC error was estimated as the standard deviation of deflection and normal strain measurements obtained from stationary pre-impact images.

A 2-by-2 full factorial completely randomized design was used to analyze the effects of MC (LMC vs. HMC) and GO (radial vs. tangential) on the mechanical properties of both species by MATLAB R2025 (MathWorks, USA) using the official Statistics and Machine Learning Toolbox. To stabilize proportional variances inherent to timber testing under varying moisture loads, raw engineering data were transformed using the natural logarithm. Prior to analysis, residual normality and variance homogeneity were verified. A two-way ANOVA test was conducted (P-value = 0.05) to evaluate the main effects and the interaction effects. Significant localized variances were subsequently isolated using Tukey's post-hoc pairwise comparisons.

Results and discussion

Table 1 summarizes the specimens' basic parameters and test results based on the MC level and species type. The presented values are the median, and in parentheses, the coefficient of variation (CV%) of the physical properties as a percentage.

Alongside the median values of different parameters, the statistical analysis is needed to specify the effect of each setting on the results. The differences in medians do not necessarily indicate statistically significant group differences, and the difference between the groups can, in fact, be negligible. Based on the group density means and variances, the observed effect size was exceptionally large (Cohen's d for ash groups and maple groups was 3.12 and 6.56, respectively). This indicates a massive physical disparity between the two wood groups that far exceeds the standard deviation of the data, thus showing that the size of the groups was big enough.

To contextualize the experimental findings, the results of the density and IBS were compared against former studies about both ash and maple wood. Table 2 presents the IBS and density of the former studies; and the difference between their results and this study for each article is shown in the parentheses. Across the cited studies, both ash and maple wood exhibited a more consistent density profile, yet their IBS values varied drastically, with the highest reported values nearly double the lowest. This suggests that for ash, density alone is a poor predictor of dynamic toughness, and the wide fluctuations in the coefficients of variation point to significant discrepancies in wood quality, grain orientation, or testing conditions among research studies.

Prior to analyzing the mechanical results, we verified the data rules for ANOVA using Table 3. For an ANOVA to be accurate, the data should follow a normal distribution shape and have suitable group spreads, with consideration of the MC and GO separations. The natural log transformation worked exceptionally well, successfully validating both rules ($p > 0.05$) for 80% of the experimental runs. There were only two minor exceptions. First, European ash deflection did not have perfectly equal spreads ($p = 0.0053$) due to natural variations in wood. However, because its data shape was highly normal ($p = 0.9442$), the ANOVA test was retained because residual distributions showed acceptable behavior. Second, sycamore maple F_{max} was slightly outside the ideal normal shape ($p = 0.0472$), but its group spreads are acceptable ($p = 0.5514$). Because the residual distributions exhibited high normality, the ANOVA framework remains robust despite the unequal sample sizes between the ash moisture groups.

The effects of MC, GO, and their interaction (MC × GO) on the impact bending characteristics of ash and maple wood are presented in Table 4. The two-way ANOVA results revealed

Table 2. Comparison of density and IBS obtained in the present study with values reported in previous studies. Values in parentheses indicate the percentage difference relative to the present study.

Study	Species	Density	IBS (J/cm²)
Kielmann et al. 2013	Ash	645 (9%)	2.6 (58%)
Brischke 2017	Ash	-	7.4 (17%)
Borůvka et al. 2020	Ash	655 (7%)	7.3 (16%)
Fortin-Smith et al. 2016a	Ash	-	5.0 (8%)
Fortin-Smith et al. 2016a	Maple	-	5.3 (16%)
Kollmann and Côté 1968	Maple	630 (2%)	6.4 (42%)
Kielmann et al. 2013	Maple	670 (4%)	3.6 (20%)
Von Wedel 1964	Maple	600 (7%)	5.2 (16%)
Sell 1968	Maple	635 (1%)	6.4 (42%)
Wagenführ 2007	Maple	630 (2%)	6.5 (44%)

Table 3. Validation of ANOVA assumptions using Levene's test for homogeneity of variance and normality tests for the log-transformed data.

Column1	Ash		Maple	
	Levene	Normality	Levene	Normality
Max Def	0.0053	0.9442	0.1684	0.8061
Max strain	0.2368	0.7907	0.7074	0.9781
F_{max}	0.1662	0.3892	0.5514	0.0472
Absorbed energy	0.2389	0.9040	0.3752	0.7284
IBS	0.1828	0.7565	0.7046	0.6045

Table 4. Results of the two-way ANOVA evaluating the effects of MC, GO, and their interaction (MC × GO) on the mechanical properties.

Material and metric	Source of variation	df	Mean square (MS)	F-value	p-value	Significance
Ash deflection	MC	1	0.0040	0.2865	0.5955	ns
	GO	1	0.0007	0.0502	0.8239	ns
	MC*GO	1	0.0173	1.2472	0.2709	ns
Maple deflection	MC	1	0.3302	6.9155	0.0142	*
	GO	1	0.0004	0.0078	0.9301	ns
	MC*GO	1	0.0111	0.232	0.6341	ns
Ash max strain	MC	1	0.0043	0.3805	0.5408	ns
	GO	1	0.0174	1.5508	0.2203	ns
	MC*GO	1	0.0020	0.1752	0.6778	ns
Maple max strain	MC	1	0.3290	4.9986	0.0342	*
	GO	1	0.0019	0.0285	0.8672	ns
	MC*GO	1	0.0014	0.0211	0.8856	ns
Ash F_{max}	MC	1	0.1967	33.1742	< 0.0001	***
	GO	1	0.1426	24.0591	< 0.0001	***
	MC*GO	1	0.0417	7.0272	0.0114	*
Maple F_{max}	MC	1	7.9241	387.071	< 0.0001	***
	GO	1	0.0077	0.3753	0.5454	ns
	MC*GO	1	0.0026	0.1289	0.7224	ns
Ash absorbed energy	MC	1	0.0070	0.2604	0.6125	ns
	GO	1	0.0928	3.434	0.0709	ns
	MC*GO	1	0.0514	1.9023	0.1751	ns
Maple absorbed energy	MC	1	0.4047	4.1808	0.0511	ns
	GO	1	0.0116	0.1202	0.7316	ns
	MC*GO	1	0.0184	0.1902	0.6663	ns
Ash IBS	MC	1	0.0888	3.1771	0.0819	ns
	GO	1	0.0896	3.2039	0.0807	ns
	MC*GO	1	0.0539	1.9259	0.1725	ns
Maple IBS	MC	1	0.0479	0.6689	0.4212	ns
	GO	1	0.0035	0.0494	0.8259	ns
	MC*GO	1	0.0937	1.3082	0.2635	ns

Significance indicators are as ns = $p \geq 0.05$, * = $p < 0.05$, ** = $p < 0.01$, and *** = $p < 0.001$.

that most of the investigated parameters were not significantly affected by MC, GO, or their interaction. For ash wood, maximum deflection and maximum strain showed no significant influence of any investigated factor ($p > 0.05$). In contrast, F_{max} was significantly affected by both MC and GO, with highly significant effects observed for MC ($F = 33.174$, $p < 0.0001$) and GO ($F = 24.059$, $p < 0.0001$). Additionally, a significant interaction between MC and GO was observed for F_{max} ($F = 7.027$, $p = 0.0114$), indicating that the influence of MC on the maximum force depended on the GO. Absorbed energy and IBS of ash wood were not significantly affected by the studied factors, although GO showed a tendency toward influencing these properties ($p = 0.0709$ and $p = 0.0807$, respectively).

For maple wood, MC significantly influenced maximum deflection ($F = 6.916$, $p = 0.0142$) and maximum strain ($F = 4.999$, $p = 0.0342$), while GO and the MC × GO interaction had no significant effects on these parameters. Similar to ash wood, F_{max} was strongly affected by MC ($F = 387.071$, $p < 0.0001$), whereas GO and the interaction effect were not significant. The effects of MC, GO, and their interaction on absorbed energy and IBS were statistically insignificant for maple wood ($p > 0.05$), although MC showed a marginal effect on absorbed energy ($F = 4.181$, $p = 0.0511$). Overall, MC was identified as the dominant factor affecting the maximum force response of both wood species, whereas its influence on energy absorption and impact bending strength was statistically insignificant. GO contributed mainly to the maximum force response of ash wood.

The contrasting impact behaviors of European ash and sycamore maple are not only due to density alone, but are also rooted in their distinct microstructural structures. European

ash features a ring-porous anatomical structure characterized by heavily densified latewood bands with a high fiber-to-parenchyma ratio. Under rapid impact stress, these dense fiber matrices can act as critical crack-arresting barriers. Conversely, sycamore maple possesses a diffuse-porous structure with smaller, uniformly distributed vessels, a lower fiber ratio, and prominent wood rays. These fundamental differences between the structures, can have a great effect on the impact response of wood. This requires a more comprehensive further study that includes the micro assessment of the structures of each specimen, alongside its impact response.

The mechanical response of both species is heavily influenced by the transition through the FSP. In the LMC groups, the presence of bound water within the cell walls acts as bonding water between wood polymers. On the other hand, the MC in both HMC groups significantly exceeded the FSP. At this stage, the cell walls are fully saturated and plasticized, and any additional moisture exists as free water in the cell lumens, which does not further reduce the strength of the cell wall matrix. The pattern of increasing MC more than FSP can be seen in former studies (Hassan Vand et al. 2024; Hassan Vand and Tippner 2024a, 2024b) where IBS, maximum deflection, and maximum strain increased with elevated MC, while maximum force drastically decreased.

The values of the maximum normal strain and deflection measured by DIC are shown in Figures 2 and 3 as boxplots. The center horizontal line within each box denotes the median value, while the (×) marker represents the sample mean. The box boundaries define the interquartile range (IQR) from the 25th to the 75th percentile. The whiskers extend to the maximum

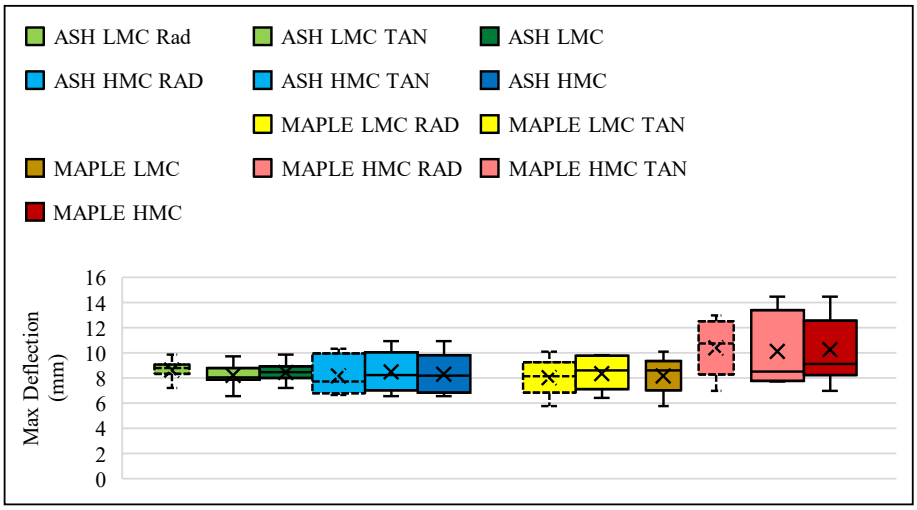


Figure 2. Maximum mid-span deflection measured by DIC up to crack initiation for both species under different MC and GO.

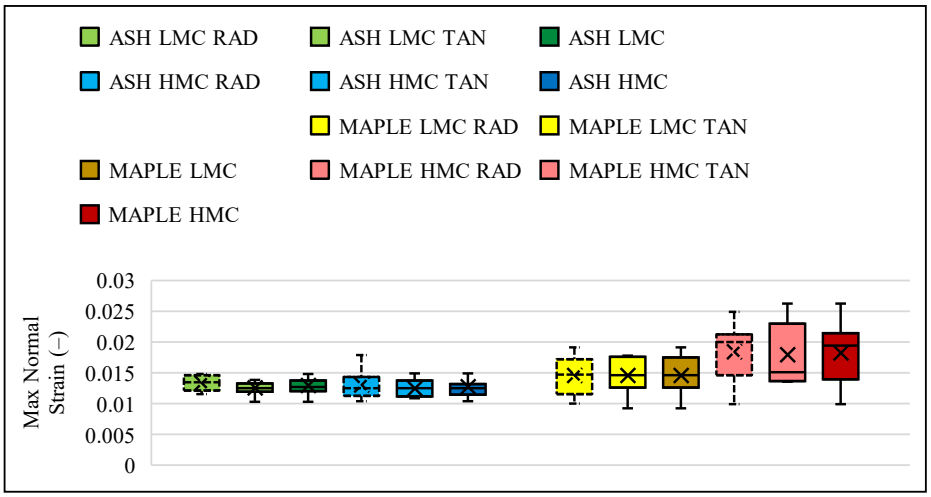


Figure 3. Maximum normal strain measured by DIC up to crack initiation for both species under different MC and GO.

and minimum data points within 1.5 IQR from the box edge; individual data points falling beyond this range are plotted as distinct outlier dots. From Figure 2, it can be seen that the ash deflection is unaffected by increasing MC. In contrast, for the maple, the increase in the MC significantly increases the flexibility. The GO also showed no influence over the flexibility of both species for both MC levels. The maximum normal strain has almost the same pattern as the maximum deflection. The maximum deflection for LMC of both species was similar, while for HMC, the ash showed no difference, whereas the maple showed improvement in deflection.

Figure 4 displays the maximum reaction force of the specimens. Boxplot parameters such as the median, mean, IQR, and whiskers follow the definitions established in Figure 2. It is clear that an increase in MC consistently decreases the maximum force for all specimens, while GO generally had no influence on the maximum force for either species at both MC levels, except for ash HMC. Notably, the effect of MC on ash, with 16% decrease, was far less pronounced compared to its effect on maple wood, with 64% decrease of the F_{max}.

Figures 5 and 6 display the median of all charts for reaction forces vs. time of all groups. To highlight their similarities and differences, the median values for the LMC and HMC groups of both species are plotted side by side.

The dynamic impact response of both ash and maple wood specimens can be distinctly categorized into three sequential chronological stages. During Stage I (0 to 0.001 s), initial contact with the impact hammer induced a rapid, highly oscillatory force peak dominated by inertial shock waves passing through the specimen and test fixtures, which subsequently stabilized into a linear elastic trend. As loading transitioned into Stage II (0.001 to 0.0025 s), the curves diverged sharply based on MC, capturing progressive micro-cracking and fiber fracture. LMC specimens climbed to a drastically high, sharp peak indicative of a rigid, brittle matrix, before experiencing sudden force drops from unstable macro-crack propagation; whereas

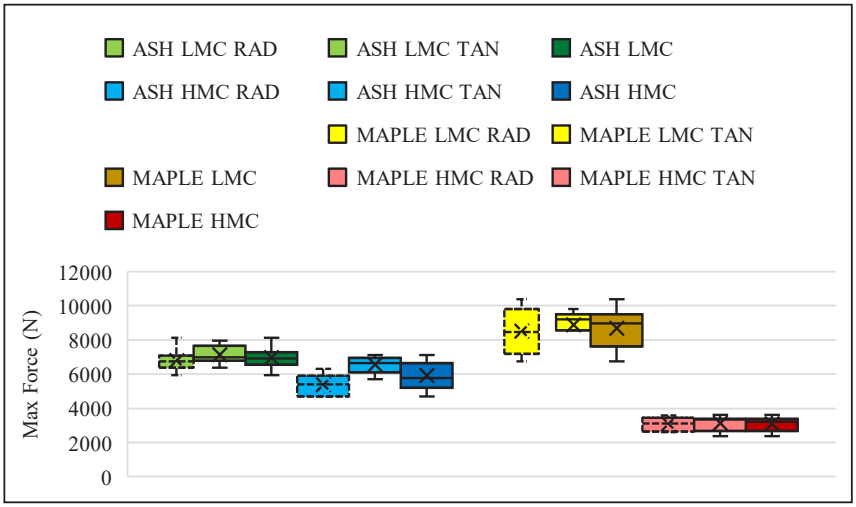


Figure 4. The maximum reaction force of the species as measured by the testing machine.

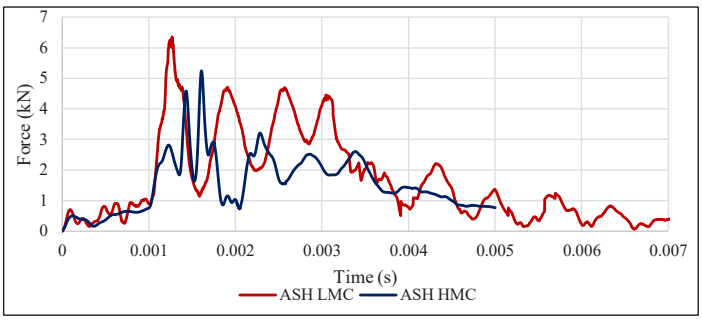


Figure 5. Median reaction force-time curves for ash specimens under low and high moisture contents. Curves represent the synchronized median responses obtained from all impact tests.

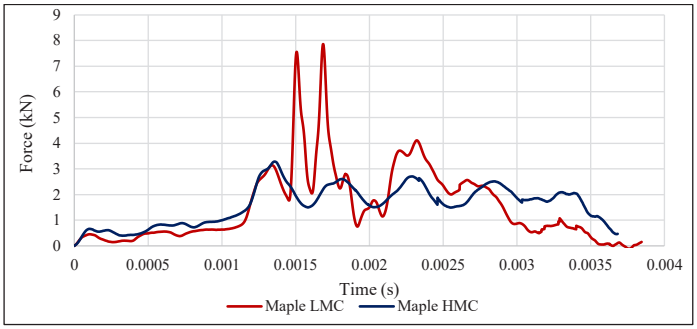


Figure 6. Median reaction force-time curves for maple specimens under low and high moisture contents. Curves represent the synchronized median responses obtained from all impact tests.

HMC specimens displayed significantly attenuated, smoother, and temporally delayed peaks representing a compliant, ductile failure mode. Finally, Stage III (0.0025 to the end) represents the post-peak degradation phase where load-bearing capacity decayed as macro-cracks fully cleaved the cross-section; here, LMC curves continued to show high-frequency force oscillations from splintering and friction, while the HMC curves decayed much more smoothly due to the structural damping qualities of the moisture-saturated cellular matrix.

The sharp contrast between the brittle failure of LMC specimens and the ductile response of HMC specimens highlights a vital safety trade-off. While LMC timber achieved significantly higher peak load capacities, its failure was instantaneous and catastrophic, offering no visual or structural warning signs. Conversely, while HMC timber had smaller peak strength, its prolonged deformation and smoother post-peak degradation provided a more compliant, progressive failure mode. In structural applications exposed to sudden impact risks (such as protective barriers, seismic-resistant designs, or rockfall shelters), a predictable, ductile deformation mode is often preferred over sudden, brittle snapping.

The primary strength-related parameter in impact loading is the amount of absorbed energy, or its dimensionless counterpart, IBS. Figures 7 and 8 illustrate the absorbed energy and IBS for all groups. Boxplot parameters such as the median, mean, IQR, and whiskers follow the definitions established in Figure 2.

Figure 7 reveals that ash generally exhibited a higher total absorbed energy than maple, and interestingly, MC had no significant effect on the ability of ash to absorb inflicted energy. Conversely, maple demonstrated a lower capacity to absorb energy, though increasing its MC marginally improved this capacity.

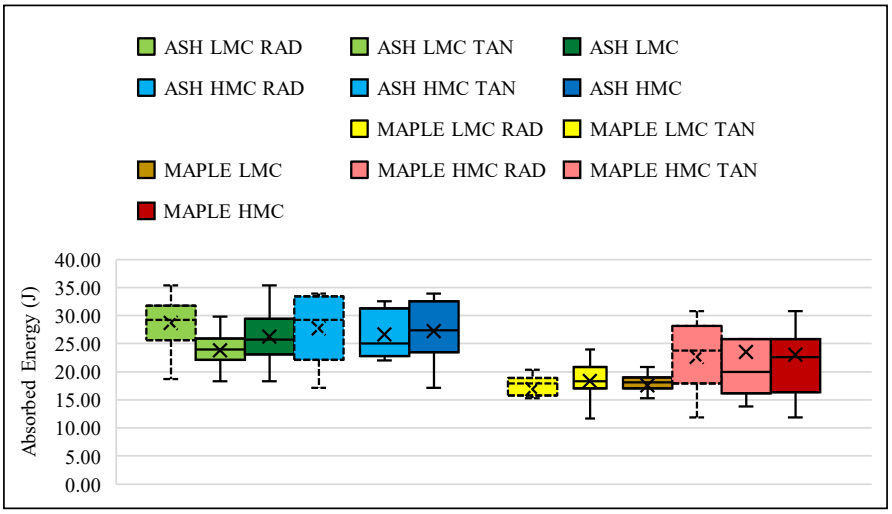


Figure 7. The absorbed energy of the species.

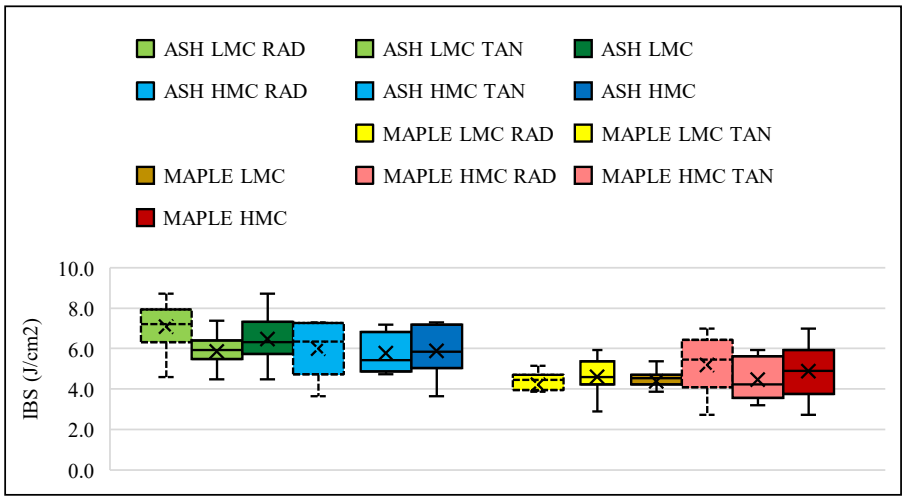


Figure 8. The IBS of the species.

Figure 8 presents the IBS values for the groups. It is important to note that the difference between IBS and absorbed energy arises from the cross-section of the specimens. Specifically, the cross-section of ash and maple specimens increased by 14% and 8%, respectively, with increased MC. This means the specimens' MC can considerably alter IBS values without affecting the absorbed energy. For example, the IBS of ash-HMC was lower than that of ash-LMC, even though the total absorbed energy of ash-HMC was higher than that of ash-LMC.

The strain distribution of each group was measured, and the strain distributions are presented in Figures 9 to 12. These strain distribution patterns can be used for validating the respective models. Both the normal and shear strain distributions were determined at 4 mm deflection. The figures reveal a symmetrical normal strain distribution. For the normal strain, the map displays the normal strain distribution illustrating compressive behavior at the top edge (purple/blue) and tensile behavior at the bottom edge (red). The highest compressive strain was observed under the impact region, close to the hammer. Conversely, the highest tensional strain, where cracks invariably initiate, was located in the central region, at the bottom of the sample. For shear strain, peaks were near the neutral axis and concentrated in the regions between the central impact hammer and the outer support grips. The distribution

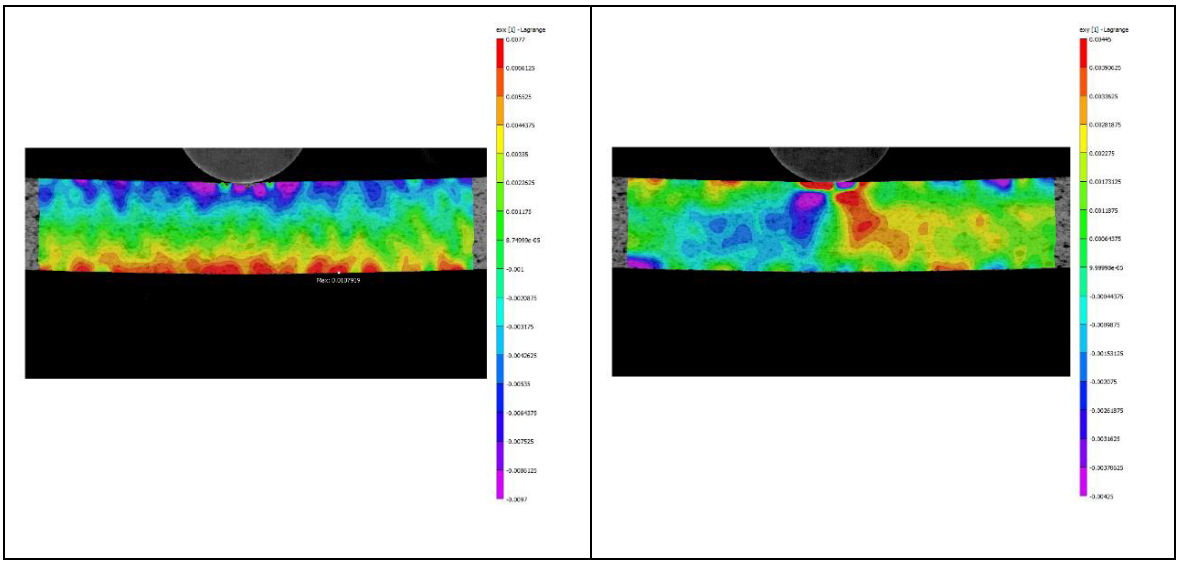


Figure 9. Representative strain distributions (DIC maps) for ash LMC specimens at a 4 mm mid-span deflection.

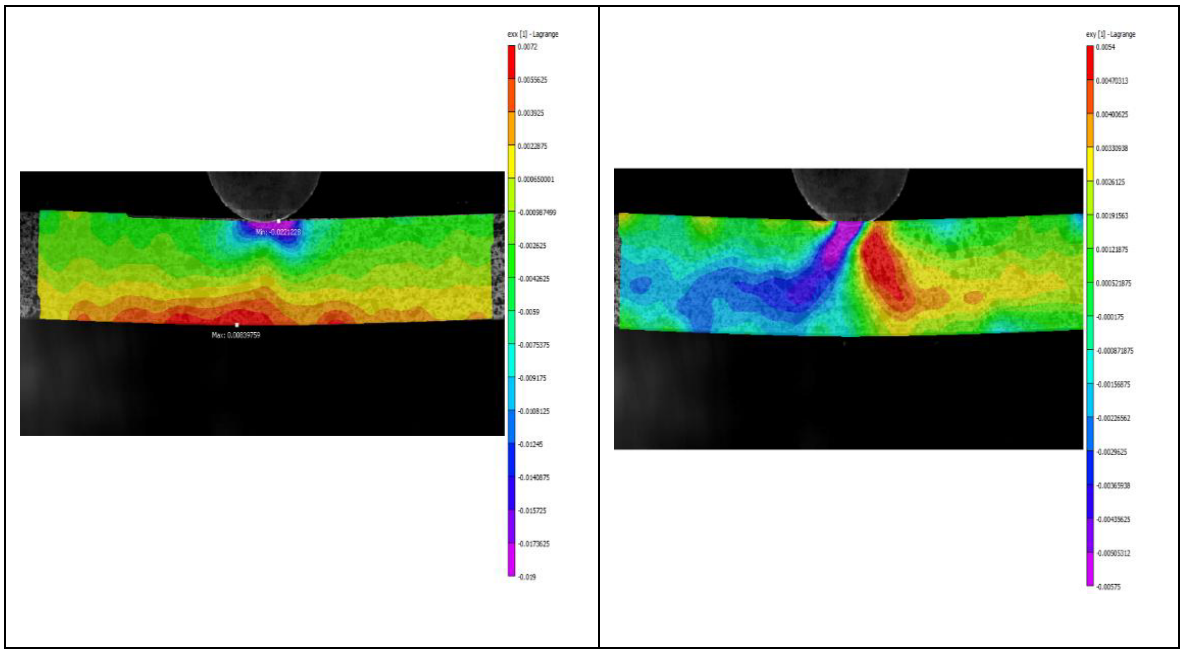


Figure 10: Representative strain distributions (DIC maps) for ash HMC specimens at a 4 mm mid-span deflection.

typically shows a clear anti-symmetric pattern, with positive and negative shear gradients splitting down the center line of the impact point. The displayed maps are taken from a single representative specimen chosen because its maximum peak force and symmetrical pattern matched the calculated median values of that group.

The shear strain distribution along the neutral axis was also determined using DIC, as shown in Figure 13. Figure 14 further illustrates the "maximum absolute shear strain" on the neutral axis of the beams. Boxplot parameters such as the median, mean, IQR, and whiskers follow the definitions established in Figure 2.

Along the neutral axis of the specimen, the shear strain distribution exhibited a highly distinct, anti-symmetric profile across the span as the material approached crack initiation. The shear strain peaks in the positive direction at between the outer support grips and the central loading point, rapidly dropped through zero directly beneath the central impact hammer, and reached a corresponding negative peak on the opposite symmetrical point. This sharp inversion from positive to negative shear gradients highlights the intense localized shear concentrations driving material deformation right before failure. Furthermore, the higher MC in the HMC specimen yielded visibly higher peak shear strain values compared to the LMC specimen, indicating

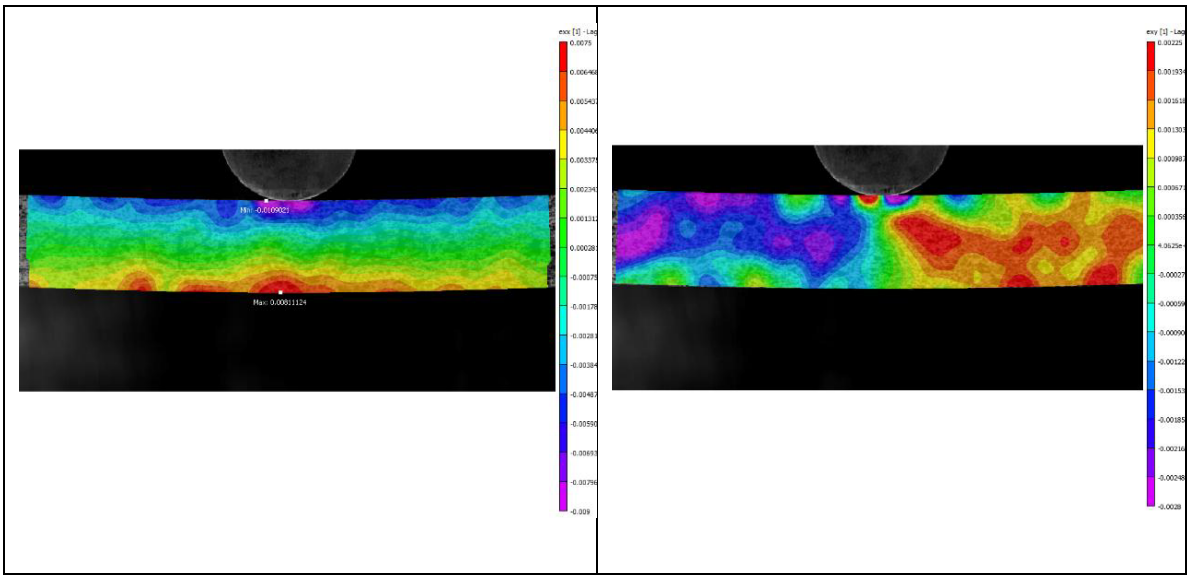


Figure 11. Representative strain distributions (DIC maps) for maple LMC specimens at a 4 mm mid-span deflection.

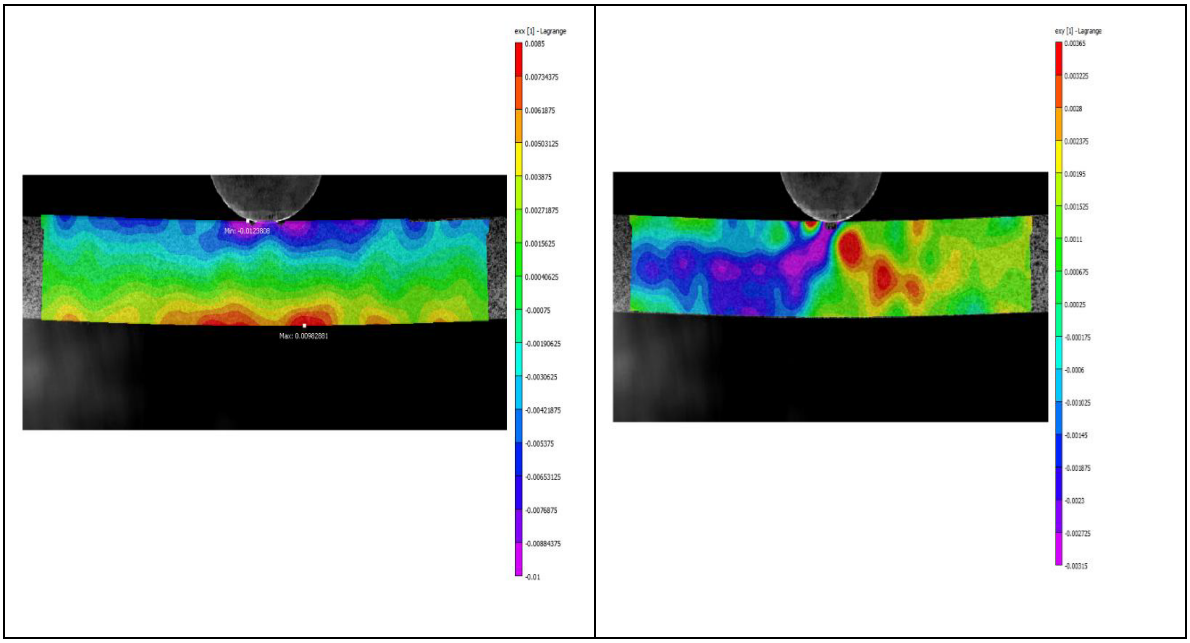


Figure 12. Representative strain distributions (DIC maps) for maple HMC specimens at a 4 mm mid-span deflection.

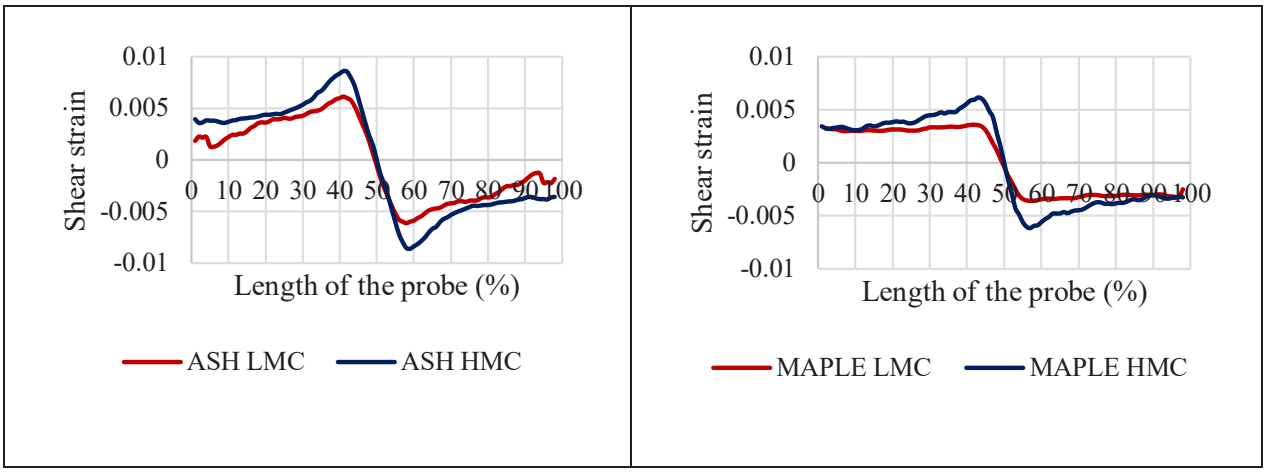


Figure 13. Shear strain distribution along the neutral axis of ash and maple beams across varying moisture levels.

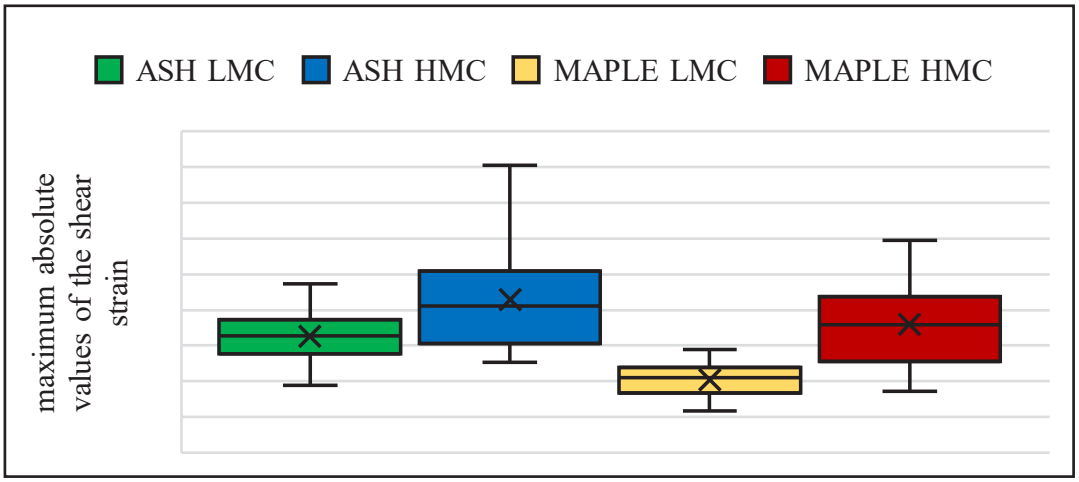


Figure 14. The maximum absolute values of the shear strain distribution over the neutral axis of the specimens.

increased material compliance and greater shear deformation prior to structural cracking.

While this study provides high-resolution insights into the dynamic behavior of European ash and sycamore maple using advanced DIC, certain limitations of this study must be acknowledged. First, the experimental design focused on two distinct moisture extremes—low moisture content, around 12% MC, and high moisture content far exceeding the FSP. Lack of assessment for other MC levels made it unable to determine the non-linear transition profiles of mechanical properties directly before, around, and after FSP. Second, while the macro-scale impact metrics and surface strain fields were successfully captured, localized internal microstructural failure mechanisms, including the influence of structural characteristics of each specimen of both species, were not investigated.

Conclusion

This research provides critical insights into the impact performance of European ash and sycamore maple, emphasizing their distinct sensitivities to moisture and GO. Consequently, a better, optimized design ultimately leads to more efficient and reliable wooden structures and products. The research confirmed ash wood's superior general impact strength and energy absorption, consistent with its widespread use in demanding applications. Notably, absorbed energy of ash remained largely unaffected by increased MC, although mechanical properties of maple, including deflection, maximum strain, and maximum force, were significantly influenced by changes in MC. The effects of GO diminished significantly in higher MC conditions for ash, while sycamore maple exhibited a more isotropic behavior regarding GO across all MC levels. The distinction between

absorbed energy and IBS was also highlighted, demonstrating that changes in specimen cross-section due to MC can independently affect IBS values, independent of total absorbed energy. The IBS of ash for lower MC levels was from 6.3 J/cm^2, whereas it reached 5.8 J/cm^2 for higher MC levels, showing an 8% decrease. For maple wood, IBS from 4.5 J/cm^2 for LMC group increased to 5.1 J/cm^2 for the HMC group, showing a 13% increase.

Another output of the study was a detailed strain distribution pattern obtained via DIC, including normal and shear strains at a certain level of deflection. Also, the shear strain of the points on the neutral axis was presented. These results offered invaluable data for validating and refining numerical models of wood behavior under dynamic loading.

The structural design of timber elements must dynamically adjust safety factors to account for moisture-induced plasticization, as high moisture content drastically degrades peak load capacity, while shifting failure from brittle to a more progressive, ductile mode. Furthermore, because GO showed negligible statistical influence on deflection, quality control in impact-critical structures should prioritize managing moisture and species thresholds over GO alignment during material selection.

Future work should further elucidate the underlying microstructural mechanisms driving these observed macroscopic responses and explore the influence of other environmental factors via tools such as X-ray computed tomography to correlate anatomical structure with impact response in areas of high deformation.

Acknowledgements

This work was supported by the Ministry of Education Youth and Sports in the Czech Republic [Grant Number #LL1909, ERC CZ].

References

Acuña L, Sepliarsky F, Spavento E, Martínez RD, Balmori JA (2020) Modelling of impact falling ball test response on solid and engineered wood flooring of two *Eucalyptus* species. Forests 11(9):933. https://www.mdpi.com/808558

Baumann G, Brandner R, Müller U, Stadlmann A, Feist F (2021) A comparative study on the temperature effect of solid birch wood and solid beech wood under impact loading. Materials 14(24):7616. https://doi.org/10.3390/ma14247616

Bodziarczyk J, Lesiński J (2011) Sycamore maple forests in Poland-a review. https://www.cabidigitallibrary.org/doi/full/10.5555/20123105506

Borůvka V, Novák D, Šedivka P (2020) Comparison and analysis of radial and tangential bending of softwood and hardwood at static and dynamic loading. Forests 11(8):896. https://www.mdpi.com/801256

Boshier D, Cordero J, Harris S, Pannell J, Rendell S, Savill P, Stewart J, Cundall N, Hubert J, Samuel S et al. (2005) Ash species in Europe: biological characteristics and practical guidelines for sustainable use. Oxford: Department of Plant Sciences, Oxford Forestry Institute, University of Oxford.

Bragov A, Igumnov L, dell'Isola F, Konstantinov A, Lomunov A, Iuzhina T (2020) Dynamic testing of lime-tree (*Tilia Europoea*) and pine (*Pinaceae*) for wood model identification. Materials 13(22):5261. https://www.mdpi.com/897314

Brischke C (2017) Interrelationship between static a Nd dynamic strength properties of wood and its structural integrity. Drvna industrija 68(1):53–60. https://hrcak.srce.hr/clanak/263383

Campshure B, Drane P, Sherwood J (2020) June. An Investigation of Maple Wood Baseball Bat Durability as a Function of Bat Profile Using LS-DYNA. In Proceedings of the 16th International LS-DYNA Users Conference (pp. 10–11). https://lsdyna.ansys.com/16th-international-ls-dyna-conference/

Choi D, Thorpe JL, Hanna RB (1991) Image analysis to measure strain in wood and paper. Wood Science And Technology 25(4):251–262. https://link.springer.com/article/10.1007/BF00225465

Czech Technical Standard (1979) ČSN 490115. Wood: Determination of ultimate strength in flexure tests. https://eshop.agentura-cas.cz/Detailnormy.aspx?k=4257

Czech Technical Standard (1979) ČSN 490117. Wood: Impact strength in flexure. https://eshop.agentura-cas.cz/Detailnormy.aspx?k=4259

Clauß S, Pescatore C, Niemz P (2014) Anisotropic elastic properties of common ash (*Fraxinus excelsior* L.). Holzforschung 68(8):941–949. https://www.degruyterbrill.com/document/doi/10.1515/hf-2013-0189/html

Dinulica F, Savin A, Stanciu MD (2023) Physical and acoustical properties of wavy grain sycamore maple (*Acer pseudoplatanus* L.) used for musical instruments. Forests 14(2):197. https://www.mdpi.com/2084164

Dobrowolska D, Hein S, Oosterbaan A, Wagner S, Clark J, Skovsgaard JP (2011) A review of European ash (*Fraxinus excelsior* L.): implications for silviculture. Forestry 84(2):133–148. https://doi.org/10.1093/forestry/cpr001

Fortin-Smith J, Sherwood J, Drane P, Kretschmann D (2016a) A Complementary Experimental and Modeling Approach for the Characterisation of Maple and Ash Wood Material Properties for the Bat/Ball Impact Modeling in LS-DYNA. In 14th International LS-DYNA Users Conference. https://lsdyna.ansys.com/14th-international-ls-dyna-conference/

Fortin-Smith J, Sherwood J, Drane P, Kretschmann D (2016b) Characterisation of maple and ash material properties as a function of wood density for bat/ball impact modeling in LS-DYNA. Procedia engineering 147:413–418. www.sciencedirect.com/science/article/pii/S1877705816307780

Fortin-Smith J, Sherwood J, Drane P, Kretschmann D (2018) Characterisation of maple and ash material properties for the finite element modeling of wood baseball bats. Appl Sci 8(11):2256. https://www.mdpi.com/366146

Gerhards CC (1977) Effect of duration and rate of loading on strength of wood and wood-based materials. USDA for serv research paper FPL 283, USDA For Serv Forest Products Laboratory, Madison, WI, United States.

Gilman FE, Watson GD (1993) *Acer pseudoplatanus* L. Sycamore Maple, Fact Sheet ST-40, USA. https://doi.org/10.32473/EDIS-ST040-1993

Glass S, Zelinka S (2021) Moisture relations and physical properties of wood. Chapter 4 in FPL-GTR-282, pp.4–1.

Gutkowski RM, Shigidi AM, Peterson ML (2007) Dynamic impact load tests of a bridge guardrail system (No. MPC Report No. 07-188). Fargo: Mountain-Plains Consortium.

Hassan Vand M, Tippner J (2023) Impact bending strength of thermally-modified timber. Holzforschung 77(11–12):828–837. https://www.degruyterbrill.com/document/doi/10.1515/hf-2023-0046/html

Hassan Vand M, Tippner J (2024a) The effect of moisture content over the fibre saturation points on the impact strength of wood. R Soc Open Sci 11(2). https://royalsocietypublishing.org/rsos/article/11/2/231685/92484

Hassan Vand M, Tippner J (2024b) Effects of moisture content on the behaviour of Scots pine heartwood and sapwood under impact. J Wood Sci 70(1):39. https://doi.org/10.1186/s10086-024-02152-2

Hassan Vand M, Tippner J, Brabec M (2024) Effects of species and moisture content on the behaviour of solid wood under impact. Eur J Wood Wood Prod 82(1):23–34. https://link.springer.com/article/10.1007/s00107-023-01986-9

Iliev N, Varbeva L, Alexandrov N (2022) Silvicultural aspects of the sycamore (*Acer pseudoplatanus* L.) propagation–Overview. Silva Balc 23(1):37–55. https://silvabalcanica.pensoft.net/article/82756/download/pdf/

Kielmann BC, Militz H, Mai C, Adamopoulos S (2013) Strength changes in ash, beech and maple wood modified with a N-methylol melamine compound and a metal-complex dye. Wood Res 58(3):343–350. www.woodresearch.sk/wr/201303/02.pdf

Keunecke D, Novosseletz K, Lanvermann C, Mannes D, Niemz P (2012) Combination of X-ray and digital image correlation for the analysis of moisture-induced strain in wood: opportunities and challenges. Eur J Wood Wood Prod 70(4):407–413. https://link.springer.com/article/10.1007/s00107-011-0573-8

Kollmann FFP, Côté WA (1968) Principles of Wood Science and Technology: I Solid Wood. Berlin, Heidelberg: Springer. Available at: https://doi.org/10.1007/978-3-642-87928-9

Kretschmann D (2010) Mechanical properties of wood. Wood handbook: wood as an engineering material: chapter 5. Centennial ed. General technical report FPL; GTR-190. Madison, WI: US Dept. of Agriculture, Forest Service, Forest Products Laboratory: p. 5.1–5.46., 190, pp.5–1. https://research.fs.usda.gov/treesearch/62243

Liu D, Chen Y (2010) The impact behavior of ecofriendly cellulosic fiber-based packaging composites. Wood Fiber Sci 42(4):460–466. https://wfs.swst.org/index.php/wfs/article/view/499

Moreira AP, Silveira ED, Almeida DHD, Almeida THD, Panzera TH, Christoforo AL, Rocco FA (2017) Toughness and impact strength in dynamic bending of wood as a function of the modulus of elasticity and the strength in compression to the grain. Int J Mater Eng 7(4):61–67. https://doi.org/10.5923/j.ijme.20170704.01

Niemz P, Clauss S, Michel F, Hansch D, Hansel A (2014) Physical and mechanical properties of common ash (*Fraxinus excelsior* L.). Wood Res 59(4):671–682. https://hdl.handle.net/20.500.11850/90545

Olmedo I, Bourrier F, Bertrand D, Toe D, Berger F, Limam A (2015) Experimental analysis of the response of fresh wood stems subjected to localized impact loading. Wood Sci Technol 49:623–646. https://doi.org/10.1007/s00226-015-0713-0

Pan B, Qian K, Xie H, Asundi A (2009) Two-dimensional digital image correlation for in-plane displacement and strain measurement: a review. Meas Sci Technol 20(6):062001. https://doi.org/10.1088/0957-0233/20/6/062001

Pasta S, de Rigo D, Caudullo G (2016) *Acer pseudoplatanus* in Europe: distribution, habitat, usage and threats. In: San-Miguel-Ayanz J, de Rigo D, Caudullo G, Houston Durrant T, Mauri A (Eds), European Atlas of Forest Tree Species. Luxembourg: Publ. Off. EU, p.e01665a. https://forest.jrc.ec.europa.eu/en/european-atlas/

Pautasso M, Aas G, Queloz V, Holdenrieder O (2013) European ash (*Fraxinus excelsior*) dieback–A conservation biology challenge. Biol Conserv 158:37–49. https://doi.org/10.1016/j.biocon.2012.08.026.

Polocoşer T, Kasal B, Stöckel F (2017) State-of-the-art: intermediate and high strain rate testing of solid wood. Wood Sci Technol 51:1479–1534. https://doi.org/10.1007/s00226-017-0925-6

Polocoşer T, Kasal B, Stöckel F, Li X (2018) Dynamic material properties of wood subjected to low-velocity impact. Mater Struct 51:1–16. https://doi.org/10.1617/s11527-018-1186-z

Polocoşer T, Stöckel F, Kasal B (2016) Low-velocity transverse impact of small, clear spruce and pine specimens with additional energy absorbing treatments. J Mater Civ Eng 28(8):04016048. https://ascelibrary.org/doi/abs/10.1061/(ASCE)MT.1943-5533.0001545

Sahraoui S, Lataillade JL (1998) Analysis of load oscillations in instrumented impact testing. Eng Fract Mech 60(4):437–446. https://www.sciencedirect.com/science/article/pii/S0013794498000241

Sedlar T, Šefc B, Stojnić S, Sinković T (2021) Wood quality characterisation of sycamore maple (*Acer pseudoplatanus* L.) and its utilisation in wood products industries. Croat J For Eng: Journal for Theory and Application of Forestry Engineering 42(3):543–560. https://hrcak.srce.hr/clanak/381464

Sell J (1968) *Eigenschaften und Kenngrössen von Holzarten*. Switzerland: Lignum, Schweizerische Arbeitsgemeinschaft für das Holz.

Sonderegger W, Martienssen A, Nitsche C, Ozyhar T, Kaliske M, Niemz P (2013) Investigations on the physical and mechanical behaviour of sycamore maple (*Acer pseudoplatanus* L.). Eur J Wood Wood Prod 71(1):91–99. https://link.springer.com/article/10.1007/s00107-012-0641-8

Sutton MA, Orteu JJ, Schreier H (2009) Image correlation for shape, motion and deformation measurements: basic concepts, theory and applications. Springer Science & Business Media.

Thomas PA (2016) Biological flora of the British Isles: Fraxinus excelsior. J Ecol 104(4):1158–1209. https://besjournals.onlinelibrary.wiley.com/doi/full/10.1111/1365-2745.12566

Tudor MP, Agnes MI, Szilard B (2011) Study of physical characteristics, mechanical and technological properties of wood species from the *Fraxinus* genus encountered in Romania compared to other main forestry species. Natural Resources and Sustainable Development, pp. 217–222. https://doi.org/10.31924/nrsd

Turnbull-Grimes C, Charlie WA, Gutkowski RM, Balogh J (2010) Bus-stop shelters: improved safety (phases 1 and 2). https://rosap.ntl.bts.gov/view/dot/18150

Von Wedel K (1964) *Untersuchungen über Eigenschaften, Verwertung und Verwendung des Ahornholzes*. Dissertation, Universität zu Göttingen.

Vacek S, Vacek Z, Kalousková I, Cukor J, Bílek L, Moser WK, Bulušek D, Podrázský V, Řeháček D (2018) Sycamore maple (*Acer pseudoplatanus* L.) stands on former agricultural land in the Sudetes–evaluation of ecological value and production potential. Dendrobiology (79):61–76. https://www.idpan.poznan.pl/pl/vol-79/79-61-76

Wagenführ R (2007) Holzatlas, 6th edn. Fachbuchverlag, Leipzig.

Yamada H, Tateyama K, Sasaki H, Naruke S, Kishimoto H, Yoshimoto M (2018) Impact resistance to ballistic ejecta of wooden buildings and a simple reinforcement method using aramid fabric. J Volcanol Geotherm Res 359:37–46. https://doi.org/10.1016/j.jvolgeores.2018.06.014